PHYSICAL REVIEW B **99**, 144518 (2019)

# Study of shock waves and solitons in bulk superfluid $^4$He

Xavier Buelna, Daniel Gonzalez, Adam Freund, and Jussi Eloranta
*Department of Chemistry and Biochemistry, California State University at Northridge, 18111 Nordhoff St., Northridge, California 91330, USA*

(Received 12 February 2019; revised manuscript received 8 April 2019; published 19 April 2019)

Properties of shock waves and solitons in superfluid $^4$He were studied by time-resolved shadowgraph experiments and theoretical density functional theory calculations. Pressure estimates for shock waves and the bright soliton limit (0.2 MPa) were provided and compared with the semiclassical Rankine-Hugoniot theory. Overall, the shock wave amplitude-velocity relationship was observed to be linear at least up to 175 kg/m$^3$. At high amplitudes, the shock waves decay into sound waves in the wake as well as a bright soliton train in the front. This suggests that the experimental shadowgraph data presented by Ancilotto *et al.* [Phys. Rev. Lett. **120**, 035302 (2018)] correspond to such a train structure rather than an individual bright soliton. With reference to theoretical calculations, a new approach based on an accelerating wall embedded in the liquid is proposed for generating single solitons in superfluid helium. This process is also predicted to produce dark solitons in superfluid helium, which have not yet been observed experimentally. At low soliton amplitudes, collision with an exponentially repulsive wall results in nearly lossless reflection, which is accompanied by soliton inversion from dark to bright or bright to dark.

DOI: 10.1103/PhysRevB.99.144518

## I. INTRODUCTION

Solitons are localized, nonlinear waves in a medium that do not disperse as a function of time and exhibit no discernible interaction during a two-wave collision [1]. These properties are distinctly different from shock waves, which, on the contrary, are highly dispersive and interact strongly during collisions. In general, solitons and shock waves can be created through various processes that invoke the nonlinear response of the medium (e.g., rapid compression of a liquid, transmission of high-intensity light in optical fibers, and acceleration of jets to supersonic or hypersonic velocities). For both solitons and shocks, a distinct relationship exists between their amplitude and propagation velocity: the higher the amplitude, the faster the nonlinear wave propagates. While the initial discovery of solitons in water by John Scott Russell dates back to the 1800s [2], in recent times solitons have found important applications, for example, in plasma physics, geophysics, geology, electronics, biology, and optics [1]. From a theoretical perspective, solitons can be described mathematically in terms of model-dependent, nonlinear partial differential equations (e.g., the nonlinear Schrödinger equation). Shock waves are often analyzed by employing the semiempirical Rankine-Hugoniot theory or its extension that is applicable in the superfluid phase [3,4]

In addition to classical media, solitons have also been observed in quantum media such as thin $^4$He films adsorbed on solid substrates at low temperatures, Bose-Einstein condensates (BECs), and $^3$He (magnetic solitons) [5–14]. For example, when a thin $^4$He film (typically only a few atomic layers thick) is driven by a sufficiently large amplitude excitation, its response becomes nonlinear (i.e., nonlinear third sound) and it has been observed to follow the Korteweg-de Vries (KdV) equation [15–19]. The distinct differences between such thin films and the bulk liquid are the dimensionality (2D vs 3D) and the presence of the film supporting substrate. The liquid-substrate interaction influences the sound velocity as a function of depth, which makes the application of a KdV-type equation attractive [16,17].

Experimental studies of nonlinear excitations in bulk superfluid helium are scarce where most experiments have concentrated on second-sound shock waves [20–22]. Previously, nonlinear first-sound shock waves have been studied in liquid helium by cryogenic compression shock tubes and recently by laser-induced plasma compression in the superfluid phase in order to characterize their transient properties (i.e., velocity, amplitude, etc.) [23–26]. On the theoretical side, formation of shock waves in superfluid helium were also noted in early density functional theory (DFT) studies of impurity solvation in superfluid helium [27,28]. As shown in a recent study, shock waves in superfluid helium evolve on a nanosecond time scale and hence time-resolved experiments are required for their characterization [26]. Recently, bright solitons were finally observed in bulk superfluid $^4$He, which were formed as a by-product of high-amplitude shock wave decay [29].

For solitons in BECs, the experimental observations have been successfully modeled by using the Gross-Pitaevskii (GP) theory [30–32]. Despite this promising success, however, the GP equation is a very poor model for more dense quantum liquids such as superfluid $^4$He. In order to accurately model the atomic-scale static and dynamic response of superfluid helium, methods such as DFT must be employed. For example, the Orsay-Trento (OT) DFT can reproduce both static and dynamic responses of superfluid helium at 0 K and it has been successfully employed in many applications [33,34]. Recently, OT-DFT was also used to model soliton propagation in superfluid helium to support the experimental observations [29].

In this work, we report on the properties of shock waves and bright solitons in bulk superfluid $^4$He. We provide

2469-9950/2019/99(14)/144518(8)

experimental data for shock wave velocity decay and the amplitude-velocity decay relationship, compare these results with OT-DFT, and finally establish the soliton limit. Furthermore, this work gives mechanistic detail regarding the initial shock wave formation, subsequent shock dispersion, and finally the emergence of solitons. The theoretical calculations also consider briefly a new scheme for creating solitons, which additionally predicts the existence of dark solitons in bulk superfluid helium.

## II. EXPERIMENT

As described in more detail previously [26,29,35], our experiment used a 355 nm laser pulse (frequency tripled Continuum Minilite-II Nd-YAG laser, 9 ns pulse length) focused down to about 100 $\mu$m diameter by a 10 cm quartz lens to ablate a copper target (99.9% purity) immersed in superfluid $^4$He at 1.7 K under saturated vapor pressure (modified Oxford Variox cryostat with optical tail). Pressure inside the cryostat was determined by a capacitance manometer (MKS Baratron 622). Both rotating (approx. 0.1 revolutions per second) and stationary copper targets were employed in the experiments, but the data shown in this work were obtained for a nonrotating target. A spatial scale of 500 $\mu$m was machined onto the target for calibrating the length scale. The first laser pulse ablated the surface of the copper target to create a high-pressure expanding plasma, which subsequently produced intense compression of the adjacent liquid. The resulting liquid-density variations were visualized by the time-resolved shadowgraph method [35,36] where a diffuse laser pulse from a frequency doubled Nd-YAG laser (Continuum Surelite-II, 532 nm, 9 ns pulse length) was used as the back-light source. The timing between the ablation and back-light pulses was established by two digital delay generators (Stanford DG 535 and Berkeley Nucleonics BNC 565), which were controlled by a computer using LIBMEAS software [37]. The shadowgraph images were recorded by a monochrome charge-coupled device (CCD) equipped with global shutter (ImagingSource DMK 23U445) and 180x zoom optics with a working distance of 95 mm. For further details on the experimental setup and the advantages of using superfluid helium as a prototype system for liquid-phase optical imaging, see Refs. [35,38]. Analysis of the recorded shadowgraph images was carried out by using the Fiji software [39,40].

## III. THEORETICAL MODEL

The theoretical calculations employed the OT-DFT method for modeling shock wave and soliton dynamics in superfluid helium [33,34]. The underlying equation is a nonlinear and nonlocal time-dependent Schrödinger equation, which was solved numerically by using LIBDFT and LIBGRID libraries [41,42]. While it is common to distinguish between solitons and solitary waves in theoretical work based on the integrability of the underlying model, such criterion is not available to guide the experimental work and hence the two terms are used interchangeably in this work. In order to reach the experimental length (memory requirement) and time scales (simulation time), the problem dimension was reduced from three to one by integrating out the perpendicular symmetry coordinates. Note that this reduced-dimension problem cannot account for possible spontaneous symmetry breaking, which can only be assessed by using a true three-dimensional OT-DFT. Analytic integration yields the following effective one-dimensional (1D) kernels for the OT functional (for notation, see Ref. [34]):

$$\bar{\Pi}_h(z) = \begin{cases} \frac{3}{4h^3}(h^2 - z^2), & \text{when } |z| \leqslant h, \\ 0, & \text{otherwise}, \end{cases} \tag{1}$$

$$\bar{V}_{\mathrm{LJ}}(z) = \begin{cases} 2\pi\epsilon\sigma^6(2\sigma^6 - 5z^6), & \text{when } z \geqslant h, \\ 2\pi\epsilon\sigma^6(2\sigma^6 - 5h^6), & \text{otherwise}, \end{cases} \tag{2}$$

$$\bar{F}(z) = \frac{1}{\sqrt{\pi}l} e^{-z^2/l^2}, \tag{3}$$

$$\bar{V}_j(z) = \pi\left[\frac{1}{\alpha_1}\left(\gamma_{11} + \gamma_{12}\frac{1+\alpha_1 z^2}{\alpha_1}\right)e^{-\alpha_1 z^2} + \frac{1}{\alpha_2}\left(\gamma_{21} + \gamma_{22}\frac{1+\alpha_2 z^2}{\alpha_2}\right)e^{-\alpha_2 z^2}\right], \tag{4}$$

where $\tilde{\Pi}_h$ is the 1D spherical average function with radius $h = 2.1903$ Å, $\tilde{V}_{\mathrm{LJ}}$ is the effective truncated Lennard-Jones potential with $\epsilon = 10.22$ K and $\sigma = 2.556$ Å, $\tilde{F}$ is the extent of the kinetic-correlation functional in 1D with $l = 1$ Å, and $\tilde{V}_j$ determines the effective range of the backflow functional with $\alpha_1 = 1.023$ Å$^{-2}$, $\alpha_2 = 0.14912$ Å$^{-2}$, $\gamma_{11} = -19.7544$, $\gamma_{12} = 12.5616$ Å$^{-2}$, $\gamma_{21} = -0.2395$, and $\gamma_{22} = 0.0312$ Å$^{-2}$. For example, the Lennard-Jones contribution to the nonlinear OT potential is represented by the following convolution:

$$\frac{\delta E_{\mathrm{LJ}}}{\delta\rho} = \int_{-\infty}^{\infty} \tilde{V}_{\mathrm{LJ}}(|z - z'|)\rho(z')dz'. \tag{5}$$

This one-dimensional model can reproduce the known OT-DFT dispersion relation and the uniform bulk liquid energy as a function of density [34]. Note that this results in a much simpler formulation than the corresponding two-dimensional theory, which employs cylindrical symmetry [43]. This is due to the fact that the presence of the radial coordinate in 2D requires the use of Hankel rather than Fourier transformation. Since inclusion of the kinetic energy correlation and backflow terms in the OT functional were observed to not change the outcome of the calculations, the production runs excluded these terms.

The initial compression along the $z$ axis for the simulation was constructed as proposed earlier [29,44]:

$$\rho(z, 0) = \rho_0\left[1 + \frac{\Delta\rho}{\rho_0}\sin^2[\pi z\Theta_w(z)/\lambda_c]\right], \tag{6}$$

where the initial order parameter is obtained from this density profile by $\psi(z, 0) = \sqrt{\rho(z, 0)}$. The parameters entering this function are $\rho_0$ the bulk density (0.0218360 Å$^{-3}$ at 0 K), $\Delta\rho$ the average amplitude of the initial compression, $\lambda_c = 3.58$ Å, and function $\Theta_w(z) = 1$ inside the spatial window of width $w$ and zero elsewhere [29]. The latter function defines the overall width of the initial layered structure, which, in the experiments, would be created by the rapidly expanding plasma. Here we have used $w = 700$ nm to generate the initial condition for the simulations.

The time-dependent order parameter in the OT equation is discretized over a regular one-dimensional grid, which had a spatial step length of 0.1 Å. The time propagation was achieved by the predictor-corrector method [45,46] with a time step length of 0.1 fs. These unusually short spatial and temporal step sizes were required due to the presence of strong nonlinearities in the calculation (i.e., shock waves and solitons) and the long simulation times required for following the soliton dynamics (nanoseconds). A typical number of grid points in the calculations was 1 310 720. Smaller three-dimensional calculations, which were used to confirm the stability of the soliton solution against symmetry breaking, employed a $512 \times 512 \times 512$ spatial grid with a step length of 0.5 Å.

The underlying Cartesian grid library uses graphics processing unit (GPU) technology in the calculations, which exploits the massively parallel capabilities of the GPU [41]. For example, the two GPUs (NVIDIA Titan V and GTX 1050 Ti) employed in this work were more than an order of magnitude faster than our reference system (64 core Opteron at 2.2 GHz). All calculations employed double precision floating point numbers in order to reach a sufficient numerical accuracy during time integration up to nanoseconds.

## IV. RESULTS

### A. Experimental results

The average wave velocity $v_{\rm av}$ is used through out this work to characterize the propagation velocity and is defined as [26]

$$v_{\rm av}(t) = \frac{1}{t}\int_0^t v_s(t')dt', \qquad (7)$$

where $t$ specifies the time up to which the average velocity is computed and $v_s(t')$ is the instantaneous velocity at time $t'$. In both experiments and simulations, $v_{\rm av}$ was determined from the ratio between the wave travel distance and the corresponding travel time. While Eq. (7) would, in principle, allow inverting the data to obtain $v_s$ as a function of time, the experimental data tend to be too noisy to obtain meaningful results. Note that this averaging process has a negligible effect on the limiting wave velocity because the long-time average overcomes the higher velocities present at the early times.

Figure 1 shows the average velocity decay of the shock wave that eventually turns into a soliton as soon as the amplitude reaches the soliton stability limit [29]. The velocity of first sound at 1.7 K is shown for reference (horizontal blue continuous line). Overall the decay appears multiexponential, but within the range shown in Fig. 1 a single exponential function can represent the data approximately. Using such a fit to extrapolate the limiting soliton velocity, a value of nearly 250 m/s would be obtained (horizontal red dashed line). In current experiments, the measured spatial width of the soliton at the convergence limit is approximately 10 $\mu$m. When the wave reflects from the walls of the cryostat, an audible sound can be heard by ear (i.e., energy dissipation), but the images do not show significant additional dispersion or amplitude reduction of the wave when they become visible again in the observation zone. This likely means that the soliton lost only a small portion of its energy during the collision. Estimates for the local pressure at the shock (or soliton) based on the zero-Kelvin OT-DFT equation of state are shown by arrows at selected points. At the convergence limit of the soliton, this estimate gives the local pressure as 0.2 MPa, which corresponds to a liquid density of $2.214362 \times 10^{-2}$ Å$^{-3}$.

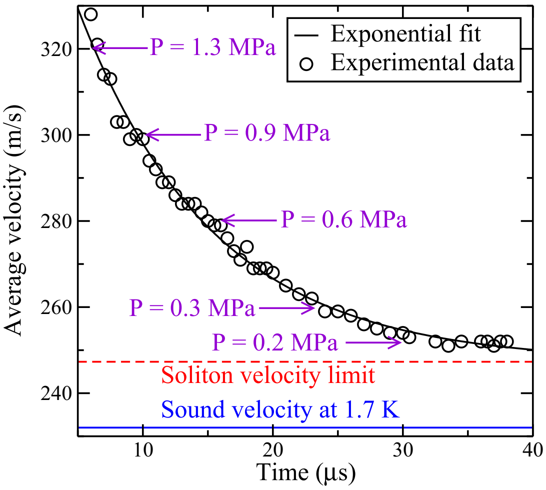

FIG. 1. Long-time average velocity of the waves (half-spherical wave; see Ref. [29] for explanation) emitted by laser ablation of copper target (0.45 GW/m$^2$) inside superfluid $^4$He at 1.7 K and saturated vapor pressure. The time axis corresponds to the delay time between the ablation and back-light laser pulses (i.e., total propagation time). The local pressure at the wave is indicated by arrows according to the OT-DFT equation of state, the asymptotic soliton regime is shown by a dashed red line, and the velocity of first sound is given for comparison as a continuous blue line.

During the shock wave velocity measurements, the wave amplitude was also determined from the contrast present in the shadowgraph images. The contrast in such images is approximately proportional to the Laplacian of liquid density (index of refraction) [36]. Since Laplacian is a linear operator, the image contrast scales correspondingly with the amplitude of the wave and hence the image contrast becomes proportional to the wave amplitude (i.e., the excess density above the bulk value). In order to eliminate the intensity fluctuations and spatial inhomogeneities present in the back-light source, we have used the undisturbed region in front of the propagating wave as reference background and subtracted it from the back-light intensity recorded at the wave. A plot of the obtained wave velocity vs relative wave amplitude is shown in Fig. 2, which exhibits initially linear dependence and then possibly nonlinear behavior emerging at higher wave amplitudes. Due to the shot-to-shot variations of the ablation laser and the unavoidable changes in the ablation target, there is inherent noise present in the experimental velocity data. As inverting Eq. (7) requires differentiation of the data, which would amplify the noise, it was not possible to perform this operation in practice. Hence, in the very beginning of the wave propagation where rapid deceleration takes place (indicated by dashed blue circle in Fig. 2), the average data are likely to be contaminated by the contribution from the past velocities. Therefore the measurement does not reflect the instantaneous velocity at early times.

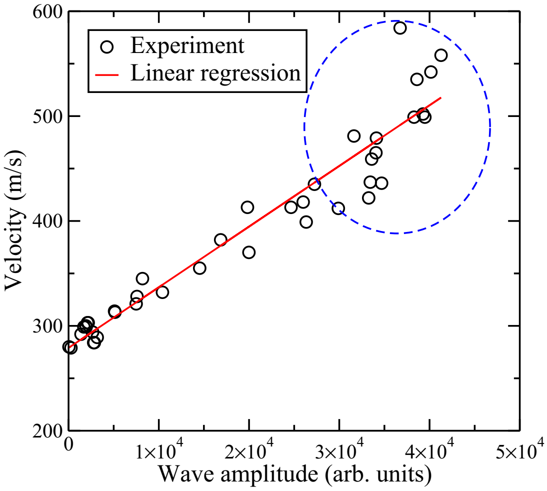

FIG. 2. Dependence of relative wave velocity on the wave amplitude for half-spherical waves created by laser ablation of copper target (0.45 GW/m$^2$) placed inside superfluid $^4$He at 1.7 K (saturated vapor pressure). The relationship appears linear with a correlation coefficient of 0.963. The region identified by a blue dashed circle corresponds to the regime where the average and instantaneous velocities may deviate significantly from each other [see Eq. (7)].

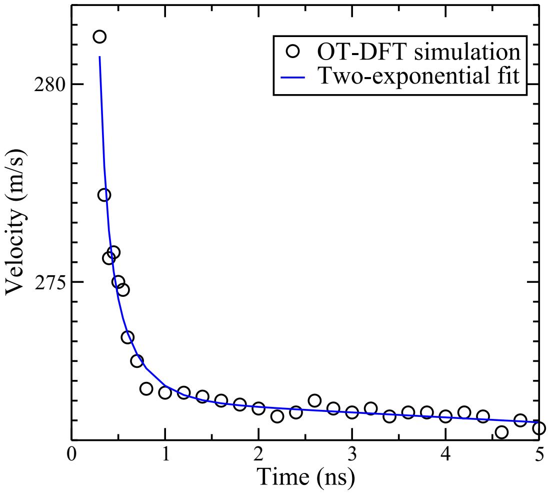

FIG. 3. Average velocity decay data for a shock wave created by using Eq. (6) with $\Delta\rho = 0.2$ as the initial density profile. A fit using two exponential functions with fast and slow decay components are shown for reference. Note that the "noise" in the simulated average velocities, which were determined by manual inspection, originates from small changes in the wave geometry as it propagates.

### B. Theoretical results

This work presents the numerical simulation of shock wave and soliton propagation in superfluid helium at the length scale similar to the recent experiments (i.e., micrometers) [29]. This was only attainable by employing the outlined one-dimensional OT-DFT model, which naturally precludes the possibility of instabilities appearing along the directions perpendicular to the wave propagation. To verify that such instabilities do not develop, we performed additional three-dimensional runs up to 500 ps in order to observe the symmetry of the wave. To understand the shock wave dynamics, we have carried out OT-DFT simulations by using Eq. (6) as the initial condition with various amplitude values ($\Delta\rho$). The resulting initial shock wave and the final soliton solution both have complicated internal structures (amplitude and phase) in the subnanometer scale, which is below the optical resolution of the experiment (microns). To concentrate on the experimentally observable features of the waves, a running average of the OT-DFT density data was performed (window width 5 nm). While the calculations can reach the experimentally relevant length scale, it is not currently possible to run the simulations for several microseconds (computational limitation). The longest OT-DFT simulations performed in this work reached up to 10 ns. The main challenges are the numerical accuracy and stability of the employed time integration scheme as well as the required computational time. The main observables recorded during the calculations were the average wave velocity and the absolute wave amplitude as a function of time. Analysis of these data also allows distinguishing between dispersive shock waves and nondispersive solitons by following the evolution of the system to the nanosecond scale.

Similar to the current and previous experimental observations [26], the initial shock wave stability was observed to decrease with increasing amplitude $\Delta\rho$ (i.e., decay in both amplitude and velocity). As an example, the average velocity data from OT-DFT calculation with an initial guess corresponding to $\Delta\rho = 0.2$ is shown in Fig. 3. Note, however, that the initial decay, which appears approximately exponential, takes place in the sub-nanosecond time scale. This is clearly much faster than the time resolution of the experiment (10 ns; limited by excitation laser and back light). A slower decay trend can also be seen in Fig. 3, which extends over the nanosecond range, but due to the limited simulation times, it is difficult to characterize this process accurately.

Within the amplitude range considered, the wave velocity vs local density at the shock follows closely the relationship for the speed of first sound for a compressed bulk liquid as demonstrated in Fig. 4. The reference bulk speed of sound was obtained from the OT-DFT equation of state at 0 K through $v_{\text{sound}} = (\partial P/\partial\rho)^{1/2}$. The reported velocity values were recorded after several nanoseconds of propagation to ensure that the average and instantaneous velocities were approximately equal. The wave position (i.e., average between front and back) was determined by hand, which introduced small uncertainties in their values.

At small initial wave amplitudes ($\Delta\rho < 0.1$), the corresponding liquid compression evolves directly into a nondispersive soliton. In contrast, at high amplitudes ($\Delta\rho = 1.0$; $\approx 173$ kg/m$^3$), a dispersive shock wave forms initially, which breaks down by leaving intense liquid excitations (sound) behind it and emits a soliton train in the front (see Fig. 5). The individual solitons were observed to be stable within the simulation time (nanoseconds).

Finally, by recognizing the fact that the rapid liquid compression produced by the laser-induced plasma leads to very complex shock wave dynamics and the emission of a soliton train, we have explored an alternative, more robust approach for creating individual solitons in superfluid helium. This

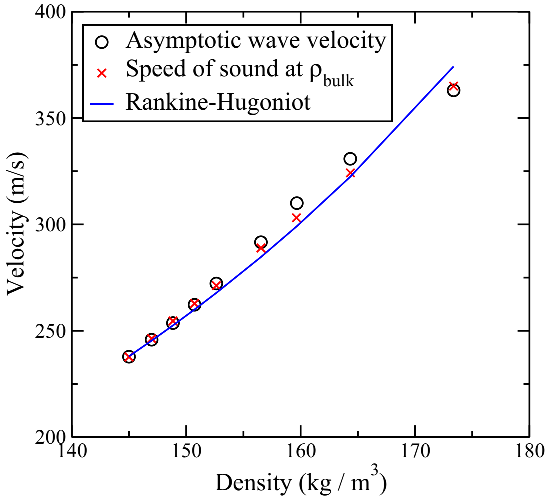

FIG. 4. Comparison between shock wave velocity at *saturated vapor pressure* and the speed of first sound in *pressurized* bulk superfluid helium based on the OT-DFT equation of state. The shock velocities and amplitudes (density) were recorded in the semistationary regime after 3 ns of propagation. The continuous blue line shows Rankine-Hugoniot results with $c_1 = 0.45$ [see Eq. (8) and the definition of $v_p$ below it].

involves first positioning a repulsive wall (e.g., a thin membrane with a large surface area) in the liquid, which is described by exponential repulsion, $A \exp[-B(z-m)]$ with $A = 3.8003 \times 10^5$ K, $B = 1.6245$ Å, and $m = 3.2$ Å. After first obtaining the equilibrium liquid density around the wall, it is then suddenly accelerated toward a specified target velocity and then stopped after a given amount of time has passed. In the simulations, this is achieved not by actually moving the wall but by changing the liquid flow velocity incident to the wall (i.e., moving the liquid background, see Ref. [47]). To demonstrate the concept using the 1D OT-DFT model, we have chosen to suddenly accelerate the flow from rest to 2 m/s for a period of 50 ps and then reset the flow velocity back to zero. Note that the wall has to be sufficiently wide such that the possible vortex emission from the edges cannot disturb the process. This procedure results in the emission of one well-defined feature on both sides of the wall. On the side toward which the wall was moved, a positive increase in liquid density takes place (compression), whereas the opposite happens on the other side (decompression). In this particular case, if the flow is kept on for longer than 50 ps, a broader continuously extending feature also appears on the high-pressure side. As illustrated by the snapshots given in Fig. 6, the two emitted waves have opposite amplitude profiles with respect to the bulk level [positive vs negative; see Fig. 6(a)], they propagate without dispersion, and they collide [Fig. 6(b)] with each other without significant change in their overall shape or amplitude [Fig. 6(c)]. As shown in the bottom part of Fig. 6, collision of these waves with the exponentially repulsive wall in the middle inverts their amplitudes [Figs. 6(d)–6(f)]. At low wave amplitudes, the collision in both cases appears lossless, but at higher amplitudes transfer of energy into shock and sound waves can be observed.

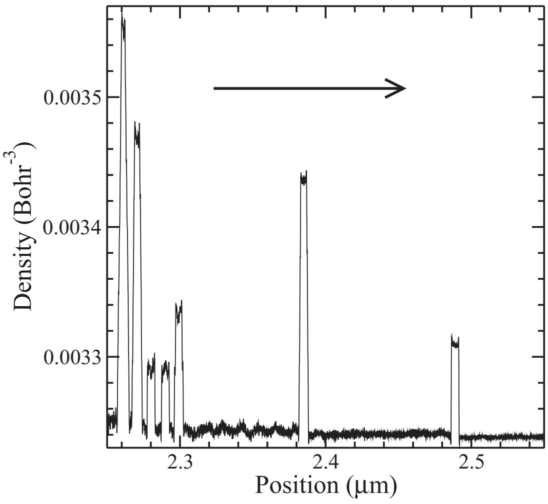

FIG. 5. Formation of soliton train from the decay of intense shock wave with initial amplitude of $\Delta\rho = 1.0$. The liquid-density snapshot corresponds to $t = 6.15$ ns with the arrow pointing in the direction of wave propagation.

## V. DISCUSSION

The shock wave velocity decay data in Fig. 1 shows a stagnant terminal velocity at about 252 m/s (speed of first sound is 238 m/s at 1.7 K and saturated vapor pressure), which is the soliton limit of the initial shock wave emitted by the rapidly expanding plasma. As shown previously by both experiments and theory, these solitary waves propagate in superfluid helium without dispersion and remain unchanged during a two-wave collision [29]. If the shock wave (or soliton) is assumed to be in thermal equilibrium with the surrounding liquid, the wave velocity can be related to the pressure (or density) at the wave (see the arrows in Fig. 1). Only after 10 $\mu$s of propagation, the internal shock pressure drops below 1 MPa with the limiting value of 0.2 MPa for the soliton regime. These values are similar to those obtained previously using Rankine-Hugoniot (RH) theory [26]. The velocity data shown in Fig. 1 appear multiexponential, especially in the initial regime (not shown). This has been previously interpreted as the presence of multiple stability regimes for the shock wave [29]. As discussed further below, similar multiexponential behavior is also seen in OT-DFT simulations.

Our experiments have determined both average velocity and relative wave amplitude as a function of time. These data are shown in Fig. 2 where linear dependence between these quantities is observed especially at low wave amplitudes. While nonlinear behavior is expected to appear at high amplitudes, this information is masked in our current experiments by the difficulty in determining the instantaneous velocities reliably [see Eq. (7)]. While this was attempted in the past to analyze the data [26], it can produce unphysical oscillations in velocity. One of the RH equations gives a relationship between the shock amplitude $\rho_s$ and propagation velocity $v_s$:

$$\frac{\rho_s}{\rho_0} = \frac{v_s}{v_s - v_p}, \tag{8}$$

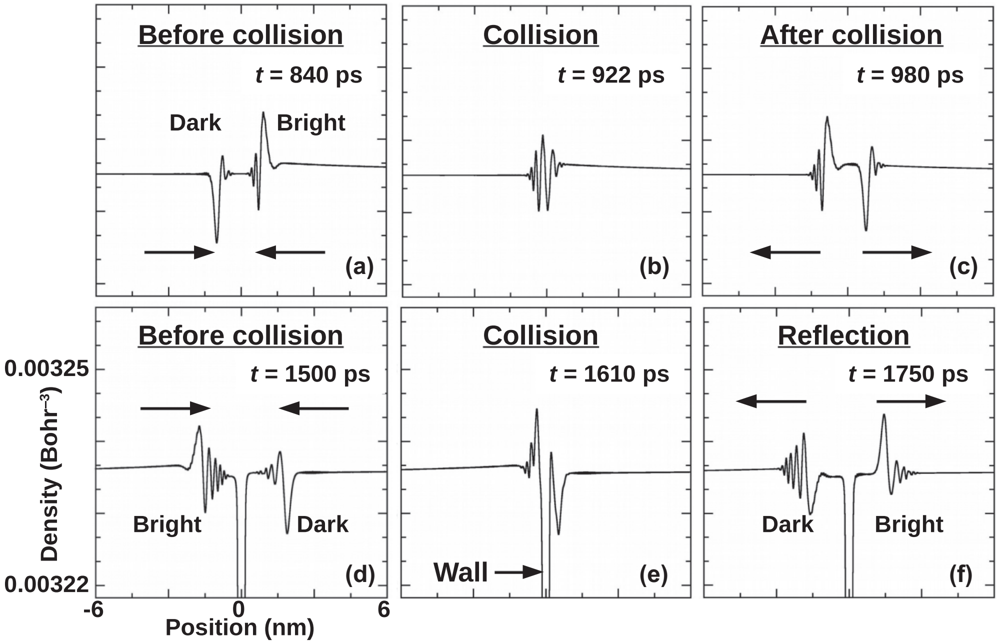

FIG. 6. Propagation, collision, and reflection of dark and bright solitons. (a) Dark and bright solitons propagate toward each other according to the arrows shown (wall not shown). (b) Dark and bright solitons collide in the middle (wall not shown). (c) Dark and bright solitons continue propagating unchanged after the collision (wall not shown). (d) Dark (right) and bright (left) solitons propagate toward the exponentially repulsive wall as shown by arrows (propagation velocities equal). (e) Both solitons collide with the wall. (f) Initially bright soliton reflects off the wall as a dark soliton and the initially dark soliton reflects as a bright soliton.

where $v_p$ is the particle velocity. The matching condition between particle velocity $v_p$ and shock velocity $v_s$ was previously determined to be linear [26], $v_p = c_1(v_s - v_0)$, where $v_0$ is the speed of first sound and $c_1 = 0.739$. This model shows that the shock velocity-density relationship should remain nearly linear to densities up to 200 $\mathrm{kg/m^3}$. However, this conclusion assumes that the matching condition itself is linear, which cannot be rigorously justified from the theoretical point of view.

Given the initial liquid compression by Eq. (6), the OT-DFT simulations show that the shock wave begins to decay exponentially within approximately 1 ns. This is followed by a slower decay in the nanosecond time scale, which cannot be reliably obtained from the current simulations. The experimentally observed decay processes take place over tens of microseconds, but as noted previously [29], these data show distinct stability regimes. It is likely that the different exponential decay times observed in the simulations represent similar stability regimes. Consequently, the simulated velocity decays appear multiexponential, which was also seen experimentally.

After letting the system relax for a couple of nanoseconds, we have determined the semistationary shock wave amplitude and velocity as shown in Fig. 4. The reference data for the speed of first sound in compressed bulk superfluid helium is shown alongside the shock wave velocity vs density data. Clearly, these two velocities appear identical within the accuracy of manual determination of the shock wave position. Thus, the shock wave propagates at the same velocity as the first sound would in a compressed bulk liquid. Therefore, by determining the shock velocity, it is possible to obtain information on the bulk liquid equation of state in the $(\rho, P)$ plane, but this leaves the shock temperature undetermined. The blue continuous line in Fig. 4 shows a least squares fit of Eq. (8) to these data where the linear matching relation was employed. This yields a value of $c_1 = 0.45$, which is considerably smaller than previously determined from experiments ($c_1 = 0.739$; see Ref. [26]). This difference may be related to the difficulty in obtaining consistent experimental data for the shock vs particle velocity data and the considerably larger pressure range (up to tens of GPa) considered in the experiments. Furthermore, it is likely that the true matching relation is not linear; but at least in the current pressure regime, the linearly matched RH equation is able to closely match the OT-DFT results.

Based on the results from the above OT-DFT simulations, it is clear that the laser ablation experiment creates an intensive shock wave, which evolves by leaving pronounced sound waves in the wake and by emitting a soliton train in the front (see Fig. 5). In fact, the former structure was observed at early times in Ref. [26] where shadows appear behind the main shock wave front. The width of the individual solitons in the train are predicted to be below the present optical resolution (several microns), which implies that, instead of observing a single soliton, multiple closely spaced solitons are likely imaged in the experiments. For this reason, we have briefly explored another scheme to produce solitons by a rapidly moving wall. Unlike the expanding plasma, such a wall has two sides, which allows studying the effect of both fast compression and decompression. In experiments, it may be possible to produce such a scenario by using piezo transducers embedded in the liquid.

An overview of dark-bright soliton collision [Figs. 6(a)–6(c)] and soliton collision with an exponentially repulsive wall are shown in Figs. 6(d)–6(f). On the side where the liquid compression took place, a nondispersive feature with its average density above the bulk level was created. Similarly, on the opposite side (decompression), localized structure with a depressed density profile results [see Fig. 6(a)]. Since these waves do not disperse and they emerge unchanged from the two-wave collision [see Figs. 6(b) and 6(c)], we assign them to be bright and dark solitons, which, in this particular exemplary case, acquired identical propagation speeds in opposite directions. During the collision, the amplitudes of the solitons cancel approximately, which implies that their main contributions must have opposite internal phases (i.e., destructive interference). By increasing the wall acceleration, the amplitudes of both solitons, and consequently their propagation velocities, can be increased accordingly.

While we have recently reported on the experimental observation of bright solitons in superfluid $^4$He [29], dark solitons in this medium have not been observed before. We note that the existence of dark solitons has been predicted previously by the Gross-Pitaevskii theory [48,49], but this model has limited applicability for modeling superfluid helium. Another interesting feature pertaining to both dark and bright solitons is their peculiar interaction with an exponentially repulsive wall. At low soliton amplitudes, there appears to be negligible changes during the collision, but the energy loss increases at higher soliton amplitudes where each collision reduces its amplitude by emitting shock and sound waves. As shown in Figs. 6(d)–6(f), the collision event also switches the identity of the soliton: bright soliton turns into dark soliton and vice versa. This is a generally known property of waves (e.g., waves on a string reflecting from a rigidly fixed point) and it has been previously observed in numerical simulations employing the nonlinear Schrödinger equation where *both* repulsive and attractive interactions are present [50]. Since OT-DFT has the short-range repulsive as well as long-range attractive terms present, this same behavior is therefore expected for superfluid helium. For the bright soliton, with its density above the bulk level, the short-range correlation terms become important, whereas for the dark soliton, the long-range attractive Lennard-Jones term takes precedence.

## VI. CONCLUSIONS

With the aid of OT-DFT calculations, we have provided pressure estimates for shock waves and the soliton limit (0.2 MPa) in superfluid helium; these estimates are in agreement with the previous analysis employing the semiempirical RH model [26]. Both experiments and theory show that the relationship between the shock wave amplitude and propagation velocity is linear at least up to a shock amplitude of 175 kg/m$^3$. At high amplitudes, OT-DFT further shows that the decay process yields both sound waves in the wake as well as a soliton train in front of the shock. Therefore, the experimental images of bright solitons presented in Ref. [29] likely correspond to multiple closely spaced bright solitons, which appear uniform due to the lack of optical resolution in the experiment. Nevertheless, such a soliton train has the exact same properties as individual solitons: it does not disperse and it shows no interaction during collision between two soliton trains. Finally, we suggest another more robust process for creating solitons in superfluid helium, which consists of a rapidly accelerating moving wall embedded inside the liquid. Such arrangement creates not only a bright soliton due to liquid compression, but also a dark soliton in the opposite low-pressure side. Both dark and bright solitons exhibit inversion during their collision with a rigid wall, which is similar to the reflection of waves.

## ACKNOWLEDGMENT

This work was supported by the National Science Foundation Grant No. DMR-1828019.

[1] P. G. Drazin and R. S. Johnson, *Solitons: An Introduction*, 2nd ed. (Cambridge University, New York, 1989).

[2] J. S. Russell, Report of the Fourteenth Meeting of the British Association for the Advancement of Science, York, September 1844 (London, 1845), pp. 311–390, Plates XLVII–LVII.

[3] M. Remoissenet, *Waved Called Solitons: Concepts and Experiments,* 3rd ed. (Springer, New York, 1999).

[4] D. M. Moody and B. Sturtevant, Phys. Fluids **27**, 1125 (1984).

[5] S. Burger, K. Bongs, S. Dettmer, W. Ertmer, K. Sengstock, A. Sanpera, G. V. Shlyapnikov, and M. Lewenstein, Phys. Rev. Lett. **83**, 5198 (1999).

[6] J. Denschlag, J. Simsarian, D. Feder, C. Clark, L. Collins, J. Cubizolles, L. Deng, E. Hagley, K. Helmerson, W. Reinhardt *et al.*, Science **287**, 97 (2000).

[7] B. P. Anderson, P. C. Haljan, C. A. Regal, D. L. Feder, L. A. Collins, C. W. Clark, and E. A. Cornell, Phys. Rev. Lett. **86**, 2926 (2001).

[8] L. Khaykovich, F. Schreck, G. Ferrari, T. Bourdel, J. Cubizolles, L. Carr, Y. Castin, and C. Salomon, Science **296**, 1290 (2002).

[9] G. Partridge, A. Truscott, and R. Hulet, Nature **417**, 150 (2002).

[10] J. Nguyen, D. Luo, and R. Hulet, Science **356**, 422 (2017).

[11] A. Marchant, T. Billiam, T. Wiles, M. Yu, S. Gardiner, and S. Cornish, Nat. Commun. **4**, 1865 (2013).

[12] C. Gould and D. Lee, Phys. Rev. Lett. **37**, 1223 (1976).

[13] V. P. Mineyev and G. E. Volovik, Phys. Rev. B **18**, 3197 (1978).

[14] K. Maki and P. Kumar, Phys. Rev. Lett. **38**, 557 (1977).

[15] M. J. McKenna, R. J. Stanley, E. DiMasi, and J. D. Maynard, Physica B **165**, 603 (1990).

[16] S. Nakajima, K. Tohdoh, and S. Kurihara, J. Low Temp. Phys. **41**, 521 (1980).

[17] S. Nakajima, S. Kurihara, and K. Tohdoh, J. Low Temp. Phys. **39**, 465 (1980).

[18] K. Kono, S. Kobayashi, and W. Sasaki, J. Phys. Soc. Jpn. **50**, 721 (1981).

[19] M. P. Lilly, F. Portier, and R. B. Hallock, Phys. Rev. B **63**, 054524 (2001).

[20] D. V. Osborne, Proc. Phys. Soc. **64**, 114 (1951).

[21] A. Y. Iznankin and L. P. Mezhov-Deglin, Sov. Phys. JETP **57**, 801 (1983).

[22] R. J. Atkin and N. Fox, J. Phys. C **18**, 1585 (1985).

[23] J. C. Cummings, J. Fluid Mech. **75**, 373 (1976).

[24] W. J. Nellis, N. C. Holmes, A. C. Mitchell, R. J. Trainor, G. K. Governo, M. Ross, and D. A. Young, Phys. Rev. Lett. **53**, 1248 (1984).

[25] H. Nagai, Ph.D. thesis, University of Tsukuba, 2000.

[26] A. Garcia, X. Buelna, E. Popov, and J. Eloranta, J. Chem. Phys. **145**, 124504 (2016).

[27] J. Eloranta and V. Apkarian, J. Chem. Phys. **117**, 10139 (2002).

[28] A. Hernando, M. Barranco, M. Pi, E. Loginov, M. Langlet, and M. Drabbels, Phys. Chem. Chem. Phys. **14**, 3996 (2012).

[29] F. Ancilotto, D. Levy, J. Pimentel, and J. Eloranta, Phys. Rev. Lett. **120**, 035302 (2018).

[30] P. G. Kevrekidis, D. J. Frantzeskakis, and R. Carretero-Gonzalez, *Emergent Nonlinear Phenomenon in Bose-Einstein Condensates: Theory and Experiment* (Springer, New York, 2008).

[31] C. Hamner, J. J. Chang, P. Engels, and M. A. Hoefer, Phys. Rev. Lett. **106**, 065302 (2011).

[32] D. K. Efimkin, J. Hofmann, and V. Galitski, Phys. Rev. Lett. **116**, 225301 (2016).

[33] F. Dalfovo, A. Lastri, L. Pricaupenko, S. Stringari, and J. Treiner, Phys. Rev. B **52**, 1193 (1995).

[34] F. Ancilotto, M. Barranco, F. Coppens, J. Eloranta, N. Halberstadt, A. Hernando, D. Mateo, and M. Pi, Int. Rev. Phys. Chem. **36**, 621 (2017).

[35] S. Sajjadi, X. Buelna, and J. Eloranta, Rev. Sci. Instr. **89**, 013102 (2018).

[36] G. S. Settles, *Schlieren and Shadowgraph Techniques* (Springer, New York, 2006).

[37] J. Eloranta, A simplified C programming interface for research instruments, Available at https://github.com/jmeloranta/libmeas/ (2018).

[38] V. Fernandez, A. Garcia, K. Vossoughian, E. Popov, S. Garrett, and J. Eloranta, J. Phys. Chem. A **119**, 10882 (2015).

[39] C. A. Schneider, W. S. Rasband, and K. W. Eliceiri, Nature Methods **9**, 671 (2012).

[40] J. Schindelin, I. Arganda-Carreras, E. Frise, V. Kaynig, M. Longair, T. Pietzsch, S. Preibisch, C. Rueden, S. Saalfeld, B. Schmid *et al.*, Nature Methods **9**, 676 (2012).

[41] L. Lehtovaara, D. Mateo, and J. Eloranta, Library for 1-D, 2-D and 3-D grids, Available at https://github.com/jmeloranta/libgrid/ (2018).

[42] L. Lehtovaara, D. Mateo, and J. Eloranta, Orsay-Trento density functional for superfluid helium, Available at https://github.com/jmeloranta/libdft/ (2018).

[43] S. L. Fiedler, D. Mateo, T. Aleksanyan, and J. Eloranta, Phys. Rev. B **86**, 144522 (2012).

[44] F. Ancilotto, F. Dalfovo, L. P. Pitaevskii, and F. Toigo, Phys. Rev. B **71**, 104530 (2005).

[45] L. L. T. Kiljunen and J. Eloranta, J. Comput. Phys. **194**, 78 (2004).

[46] L. Lehtovaara, J. Toivanen, and J. Eloranta, J. Comput. Phys. **221**, 148 (2007).

[47] A. Freund, D. Gonzalez, X. Buelna, F. Ancilotto, and J. Eloranta, Phys. Rev. B **98**, 094520 (2018).

[48] C. A. Jones and P. H. Roberts, J. Math. Phys. A **15**, 2599 (1982).

[49] N. G. Berloff and P. H. Roberts, J. Math. Phys. A **37**, 11333 (2004).

[50] W. Kim and H.-T. Moon, J. Korean Phys. Soc. **38**, 558 (2001).